# Targeting galectin-1 inhibits pancreatic cancer progression by modulating tumor–stroma crosstalk

Carlos A. Orozco[a,1], Neus Martinez-Bosch[a,1], Pedro E. Guerrero[a,2], Judith Vinaixa[a], Tomás Dalotto-Moreno[b], Mar Iglesias[c,d], Mireia Moreno[a], Magdolna Djurec[e], Françoise Poirier[f], Hans-Joachim Gabius[g], Martin E. Fernandez-Zapico[h], Rosa F. Hwang[i], Carmen Guerra[e], Gabriel A. Rabinovich[b,j,3], and Pilar Navarro[a,k,3]

[a]Cancer Research Program, Hospital del Mar Medical Research Institute, 08003 Barcelona, Spain; [b]Laboratorio de Inmunopatología, Instituto de Biología y Medicina Experimental, Consejo Nacional de Investigaciones Científicas y Técnicas, C1428ADN Buenos Aires, Argentina; [c]Department of Pathology, Autonomous University of Barcelona, 08005 Barcelona, Spain; [d]Centro de Investigación Biomédica en Red de Cáncer, Hospital del Mar, 08005 Barcelona, Spain; [e]Molecular Oncology Program, Centro Nacional de Investigaciones Oncológicas, 28029 Madrid, Spain; [f]Jacques Monod Institute, Paris Diderot University, UMR CNRS 7592, 75205 Paris Cedex 013, France; [g]Institut für Physiologische Chemie, Tierärztliche Fakultät, Ludwig-Maximilians-Universität, D-80539 Munich, Germany; [h]Schulze Center for Novel Therapeutics, Division of Oncology Research, Mayo Clinic, Rochester, MN 55905; [i]Department of Surgical Oncology, University of Texas MD Anderson Cancer Center, Houston, TX 77230; [j]Departamento de Química Biológica, Facultad de Ciencias Exactas y Naturales, Universidad de Buenos Aires, C1428 Buenos Aires, Argentina; and [k]Institute of Biomedical Research of Barcelona-Consejo Superior de Investigaciones Cientificas, 080036 Barcelona, Spain

Contributed by Gabriel A. Rabinovich, March 13, 2018 (sent for review December 26, 2017; reviewed by Juan L. Iovanna and Raul Mostoslavsky)

**Pancreatic ductal adenocarcinoma (PDA) remains one of the most lethal tumor types, with extremely low survival rates due to late diagnosis and resistance to standard therapies. A more comprehensive understanding of the complexity of PDA pathobiology, and especially of the role of the tumor microenvironment in disease progression, should pave the way for therapies to improve patient response rates. In this study, we identify galectin-1 (Gal1), a glycan-binding protein that is highly overexpressed in PDA stroma, as a major driver of pancreatic cancer progression. Genetic deletion of Gal1 in a *Kras*-driven mouse model of PDA (*Ela-Kras*$^{G12V}$*p53*$^{-/-}$) results in a significant increase in survival through mechanisms involving decreased stroma activation, attenuated vascularization, and enhanced T cell infiltration leading to diminished metastasis rates. In a human setting, human pancreatic stellate cells (HPSCs) promote cancer proliferation, migration, and invasion via Gal1-driven pathways. Moreover, in vivo orthotopic coinjection of pancreatic tumor cells with Gal1-depleted HPSCs leads to impaired tumor formation and metastasis in mice. Gene-expression analyses of pancreatic tumor cells exposed to Gal1 reveal modulation of multiple regulatory pathways involved in tumor progression. Thus, Gal1 hierarchically regulates different events implicated in PDA biology including tumor cell proliferation, invasion, angiogenesis, inflammation, and metastasis, highlighting the broad therapeutic potential of Gal1-specific inhibitors, either alone or in combination with other therapeutic modalities.**

pancreatic cancer | galectin-1 | tumor microenvironment | tumor immunity | pancreatic stellate cells

Of all solid tumors, pancreatic ductal adenocarcinoma (PDA) has the direst prognosis; in the absence of any significant advance in its treatment or early diagnosis, it is projected to become the second leading cause of cancer death in the United States by 2030 (1). In addition to late diagnosis, a major factor for this dismal prognosis is the high resistance of PDA to therapies, which has been associated to its hostile tumor microenvironment (2, 3). PDA represents a paradigm of oncogenic tumor–stroma crosstalk, as stromal components represent up to 90% of the pancreatic tumor volume and are co-opted by tumor cells to favor tumor progression. Accordingly, targeting PDA stroma has recently emerged as a promising strategy to fight against this fatal disease (4–8). Numerous studies, however, have unveiled the complexity and delicate balance between the detrimental and beneficial effects of tumor–stroma interactions in PDA (9–12).

The pancreatic tumor microenvironment contains abundant extracellular matrix proteins, endothelial cells, immune cells, and cancer-associated fibroblasts (CAFs). Activated pancreatic stellate cells (PSCs) represent most of the CAFs in pancreatic tumors and are characterized by α-smooth muscle actin (α-SMA) expression and the secretion of numerous factors favoring tumor progression (13–19). Besides the abundant presence of CAFs, the PDA stroma is also characterized by a highly immunosuppressive microenvironment, with increased numbers of regulatory cells, such as myeloid-derived suppressor cells (MDSCs), M2-type macrophages, and Foxp3$^+$ regulatory T lymphocytes (Tregs), together with a conspicuous absence of effector (CD4$^+$ and CD8$^+$) T cells. This scenario leads to profound immune evasion that might explain, at least in part, why pancreatic cancer is fully refractory to immunotherapeutic modalities (20–23).

Increasing knowledge has led to the identification of the molecular alterations responsible for PDA tumor initiation and progression. Mutations in *KRAS*, which are found in more than

## Significance

Pancreatic ductal adenocarcinoma (PDA) is the third leading of cause of cancer death in the United States and is predicted to be the second one by 2030. The tumor microenvironment is a major source of soluble mediators that influence tumor progression and hinder the success of therapeutic strategies. Using a genetically engineered mouse model and human cell-based systems, we identify galectin-1 (Gal1) as a critical soluble factor capable of regulating tumor–stroma crosstalk promoting proliferation, angiogenesis, and modulation of inflammatory responses, resulting in enhanced tumor development and metastasis. Our data provide an integrated view of the role of Gal1 in the PDA microenvironment and reinforce the high therapeutic value of Gal1 inhibition in PDA treatment.

Author contributions: C.A.O., N.M.-B., M.E.F.-Z., C.G., G.A.R., and P.N. designed research; C.A.O., N.M.-B., P.E.G., J.V., M.I., M.M., and M.D. performed research; F.P., H.-J.G., and R.F.H. contributed new reagents/analytic tools; C.A.O., N.M.-B., P.E.G., T.D.-M., M.I., M.E.F.-Z., C.G., G.A.R., and P.N. analyzed data; and C.A.O., N.M.-B., C.G., G.A.R., and P.N. wrote the paper.

Reviewers: J.L.I., INSERM U1068; and R.M., The Massachusetts General Hospital.

The authors declare no conflict of interest.



Data deposition: The gene-expression profiles by microarray analysis of RWP-1 cells untreated or treated with recombinant Galectin-1 have been deposited in the National Center for Biotechnology Information Gene Expression Omnibus (GEO) database (accession no. GSE109070).

[1]C.A.O. and N.M.-B. contributed equally to this work.

[2]Present address: Biochemistry and Molecular Biology Unit, Department of Biology, University of Girona, Campus de Montilivi, 17003 Girona, Spain.

[3]To whom correspondence may be addressed. Email: gabyrabi@gmail.com or pnavarro@imim.es.

This article contains supporting information online at www.pnas.org/lookup/suppl/doi:10.1073/pnas.1722434115/-/DCSupplemental.

Published online April 3, 2018.

90% of human PDAs, occur in the earliest steps of tumor progression (24), followed by alterations in tumor-suppressor genes, including *TP53*, *SMAD4*, and *CDKN2A* (25). Genetically engineered mouse models (GEMMs) are essential tools for studying the molecular mechanisms underlying PDA progression and for evaluating potential therapeutic targets (26). In particular, GEMMs harboring pancreas-specific mutated KRAS are currently considered the best models to mirror human pathology, as these mice develop the full spectrum of pancreatic tumor progression, from metaplastic and preneoplastic lesions to adenocarcinoma and metastasis (27–32). Moreover, tumors from *Kras*-driven mouse models of PDA present high histopathological similarities to human PDA, including abundant desmoplastic stroma (26) and a prominent immunosuppressive microenvironment (33).

Galectins are a family of glycan-binding proteins composed of 15 members with shared structural homology (34–36). Galectin-1 (Gal1), a prototype member of this family, plays major roles in cancer by modulating different processes leading to tumor progression (34–38). Several reports have shown increased Gal1 expression in human cancer, including PDA (39–42). Using a *c-myc*–driven murine PDA model, we demonstrated that this lectin exerts a broad range of protumoral effects (43). Interestingly, Gal1 expression in pancreatic tumors is expressed mostly within the stromal compartment (39, 41–43), displaying in vitro and in vivo protumoral effects (18, 44–47). However, the precise role and molecular mechanisms responsible for Gal1-mediated tumor–stroma crosstalk and their translation into the complex pathobiology of PDA are puzzling and not fully understood. We therefore sought to determine the role of Gal1 in PDA tumor progression by analyzing the biological consequences of its genetic deletion in a *Kras*-driven mouse model of pancreatic cancer (*Ela-Kras$^{G12V}$p53$^{-/-}$*). Further, using patient-derived PSCs and pancreatic cancer cells, we modeled the human PDA tumor–stroma crosstalk. These data demonstrate in vitro and in vivo that Gal1 plays a critical role in PDA progression.

## Results

**Gal1 Deletion Increases Survival in the *Ela-Kras$^{G12V}$p53$^{-/-}$* Model of Pancreatic Cancer.** The *Kras$^{+/LSLG12Vgeo}$; p53$^{lox/lox}$;Elas-tTA;TetO-Cre* (herein "*Ela-Kras$^{G12V}$p53$^{-/-}$*") transgenic model, which expresses the *Kras$^{G12V}$* oncogene in pancreatic acinar cells using an elastase-driven inducible Tet-Off strategy (48), is considered one of the best models for studying PDA in the preclinical setting, as it faithfully recapitulates the natural history and hallmarks of this disease (28, 48). *Ela-Kras$^{G12V}$p53$^{-/-}$* mice develop ductal tumors displaying abundant desmoplasia with extensive extracellular matrix protein deposition and activated α-SMA$^{+}$ positive PSCs (Fig. 1*A*). Immunohistochemical analysis for Gal1 showed high expression in the stromal compartment (Fig. 1*A*), recapitulating the pattern found in human PDA (39, 43). To determine the role of Gal1 in pancreatic tumor formation and progression, we crossed *Ela-Kras$^{G12V}$p53$^{-/-}$* mice with mice lacking the Gal1 gene (*Lgals1$^{-/-}$*). After generation of the *Ela-Kras$^{G12V}$p53$^{-/-}$Lgals1$^{+/+}$*, *Ela-Kras$^{G12V}$p53$^{-/-}$Lgals1$^{+/-}$*, and *Ela-Kras$^{G12V}$p53$^{-/-}$Lgals1$^{-/-}$* mice, we selected the *Ela-Kras$^{G12V}$p53$^{-/-}$Lgals1$^{+/+}$* and *Ela-Kras$^{G12V}$p53$^{-/-}$Lgals1$^{-/-}$* genotypes for further characterization, as Gal1 heterozygotes showed no phenotypic differences from *Lgals1$^{+/+}$* mice. *Ela-Kras$^{G12V}$p53$^{-/-}$Lgals1$^{-/-}$* mice developed ductal pancreatic tumors with histopathological hallmarks similar to those in tumors from *Ela-Kras$^{G12V}$p53$^{-/-}$Lgals1$^{+/+}$* mice (Fig. 1*A*). However, we observed a significant increase (22.3%) in the lifespan of Gal1-KO (*Lgals1$^{-/-}$*) mice (Fig. 1*B*). Interestingly, these differences became more evident when short-term and long-term survivors were compared. Specifically, 10% of *Ela-Kras$^{G12V}$p53$^{-/-}$Lgals1$^{+/+}$* mice died before 3 mo, and only 20% survived more than 6 mo. In the absence of Gal1, survival changed to 5.3% for short-term survivors (a 47% decrease) and 36.8% for long-term survivors (an 84% increase) (Fig. 1*C* and Table S1).

**Gal1 Deletion Delays Tumorigenesis and Impairs Tumor Progression in *Ela-Kras$^{G12V}$p53$^{-/-}$* Mice.** To define whether the survival phenotype observed was a consequence of delayed tumor onset and/or progression, 4-mo-old mice were killed, and tumors were analyzed. Histological characterization of pancreata showed that both *Ela-Kras$^{G12V}$p53$^{-/-}$Lgals1$^{+/+}$* and *Lgals1$^{-/-}$* mice displayed the full spectrum of PDA progression at 4 mo, including normal pancreas, acinar-to-ductal metaplasia and precursor lesions, and fully developed ductal pancreatic tumors with one or multiple nodules (Fig. 2*A*). Interestingly, *Lgals1$^{-/-}$* animals showed a less aggressive lesion distribution, characterized by an increased number of normal pancreata, precursor lesions, and uninodular tumors compared with *Lgals1$^{+/+}$* mice (Fig. 2*B*). Quantitative analysis showed a significant decrease in the number of nodules per animal in the *Ela-Kras$^{G12V}$p53$^{-/-}$Lgals1$^{-/-}$* compared with *Lgals1$^{+/+}$* mice (Fig. 2*C*). These data suggest that Gal1 expression in tumor stroma may favor PDA initiation and tumor foci development.

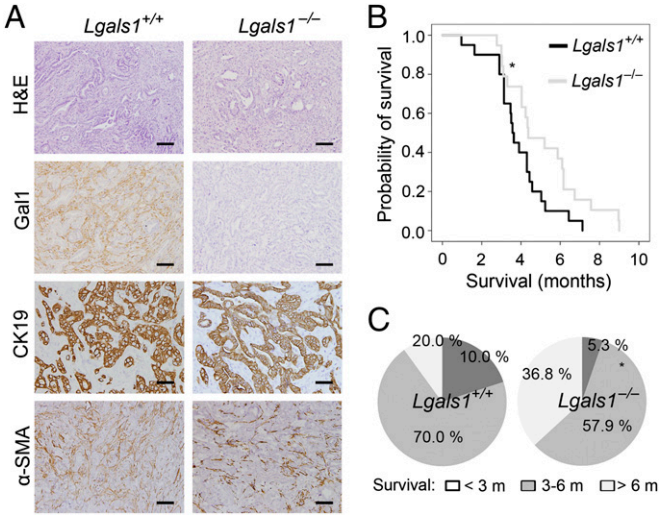


**Fig. 1.** Gal1 deficiency increases lifespan in the *Ela-Kras$^{G12V}$p53$^{-/-}$* PDA mouse model. (*A*) H&E staining and Gal1, CK19, and α-SMA IHC in tumor samples from *Ela-Kras$^{G12V}$p53$^{-/-}$Lgals1$^{+/+}$* and *Ela-Kras$^{G12V}$p53$^{-/-}$Lgals1$^{-/-}$* mice. (Scale bars: 100 μm for H&E, Gal1, and α-SMA staining and 50 μm for CK19.) (*B*) Kaplan–Meier survival curves for *Ela-Kras$^{G12V}$p53$^{-/-}$Lgals1$^{+/+}$* ($n$ = 20) and *Ela-Kras$^{G12V}$p53$^{-/-}$Lgals1$^{-/-}$* ($n$ = 19) mice. *$P$ < 0.05, log-rank test. (*C*) Pie charts showing a summary of survival data indicating animals that survived less than 3 mo (short-term), 3–6 mo, or >6 mo (long-term). *$P$ < 0.05, $\chi^2$ test.

Next, we explored the effects of Gal1 genetic ablation on PDA tumor progression by analyzing metastasis formation. One of the interesting features of the *Ela-Kras$^{G12V}$p53$^{-/-}$* model is the generation of tumor metastases located in the liver and lung, which recapitulate those observed in the human condition. Interestingly, the presence of liver metastases was significantly and selectively reduced in mice harboring *Lgals1$^{-/-}$* tumors compared with *Lgals1$^{+/+}$* mice (Fig. 2*D*). These data support a role for Gal1 in PDA initiation, progression, and metastasis.

**Gal1 Deletion Reduces Stroma Activation, Decreases Angiogenesis, and Enhances Immune Cell Recruitment in *Ela-Kras$^{G12V}$p53$^{-/-}$* Mice.** Due to the high levels of Gal1 expression in the PDA stroma and the previously reported role of this lectin in the regulation of immune and endothelial cell function (43), we sought to examine the impact of Gal1 inactivation in the tumor microenvironment. Characterization of the primary tumors developed at 4 mo by *Ela-Kras$^{G12V}$p53$^{-/-}$Lgals1$^{+/+}$* or *Ela-Kras$^{G12V}$p53$^{-/-}$Lgals1$^{-/-}$* mice revealed that Gal1-deficient mice showed significantly smaller tumors than *Lgals1$^{+/+}$* mice (Fig. 3*A*). Immunohistochemical analysis showed that the decreases in tumor weight were not associated with impaired proliferation or increased tumor apoptosis or necrosis (Fig. S1*A*). However, *Ela-Kras$^{G12V}$p53$^{-/-}$* tumors that developed in the absence of Gal1 showed impaired stroma activation and decreased tumor vascularization

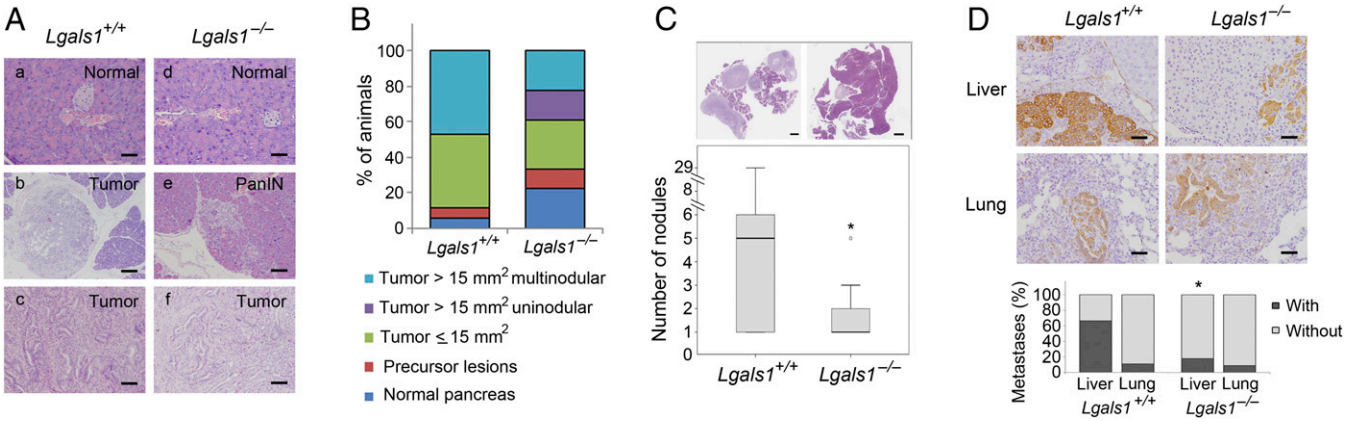


**Fig. 2.** Analysis of pancreatic lesions from 4-mo-old *Ela-Kras*$^{G12V}$*p53*$^{-/-}$*Lgals1*$^{+/+}$ or *Ela-Kras*$^{G12V}$*p53*$^{-/-}$*Lgals1*$^{-/-}$ mice. (*A*) H&E-staining characterization of normal pancreas (*a* and *d*) and preneoplastic (*e*) and tumor (*b*, *c*, and *f*) lesions found in 4-mo-old *Ela-Kras*$^{G12V}$*p53*$^{-/-}$*Lgals1*$^{+/+}$ and *Ela-Kras*$^{G12V}$*p53*$^{-/-}$*Lgals1*$^{-/-}$ mice. (Scale bars: 50 μm in *a* and *d*, 20 μm in *b*, and 100 μm in *c*, *e*, and *f*.) (*B*) Bar chart showing the percentage of mice with different types of lesions at 4 mo, when *Ela-Kras*$^{G12V}$*p53*$^{-/-}$*Lgals1*$^{+/+}$ ($n = 17$) and *Ela-Kras*$^{G12V}$*p53*$^{-/-}$*Lgals1*$^{-/-}$ ($n = 18$) mice were killed. Animals were classified according to the highest histological grade lesion observed. (*C*) Representative images (*Upper*) and number of nodules in each tumor (*Lower*). (Scale bars: 1 mm.) $^*P < 0.05$. (*D*, *Upper*) Liver and lung pancreatic metastases stained with anti-CK19 antibody. (*Lower*) Quantification showing the percentage of mice with metastases. (Scale bars: 50 μm.) $^*P < 0.05$ ($\chi^2$ test).

(Fig. 3*B* and Fig. S1*B*), which could, at least in part, contribute to the reduction of tumor size.

Given the well-established role of Gal1 in immune evasion (35, 49), we also considered the possibility that decreased tumor size after Gal1 deletion could be associated with altered frequency of effector versus regulatory immune cells. We thus analyzed tumor-associated immune cell infiltrates from *Ela-Kras*$^{G12V}$*p53*$^{-/-}$*Lgals1*$^{+/+}$ or *Lgals1*$^{-/-}$ tumors by flow cytometry. Tumor infiltrates from *Ela-Kras*$^{G12V}$*p53*$^{-/-}$*Lgals1*$^{+/+}$ mice showed a paucity of infiltrating T cells and a high proportion of myeloid cell populations (Fig. 3*C*). In contrast, *Ela-Kras*$^{G12V}$*p53*$^{-/-}$*Lgals1*$^{-/-}$ tumors were accompanied by an increased frequency of T lymphocytes (CD45$^+$ CD3$^+$) (Fig. 3*C*). Detailed analysis of T-cell subsets revealed that the numbers of CD4$^+$ T cells and CD8$^+$ cytotoxic T cells were enriched in Gal1-KO tumors compared with *Ela-Kras*$^{G12V}$*p53*$^{-/-}$*Lgals1*$^{+/+}$ tumors (Fig. 3*C*). These data were confirmed by immunohistochemical analysis of immune cell infiltrates (Fig. S2*A*). Of note, Tregs were rarely found in either *Lgals1*$^{+/+}$ or *Lgals1*$^{-/-}$ tumors, as shown by Foxp3 staining (Fig. S2*B*). Finally, changes in immune cell infiltrates were not restricted to only the lymphoid lineage, as the proportion of CD11b$^+$Gr1$^+$ MDSCs was strongly reduced in *Ela-Kras*$^{G12V}$*p53*$^{-/-}$*Lgals1*$^{-/-}$ tumors (Fig. 3*C*). Thus, Gal1 could effectively promote an immunosuppressive microenvironment impairing lymphocyte infiltration and facilitating MDSCs expansion.

Together, these results point to a key role for Gal1 in PDA tumorigenesis and progression in the *Ela-Kras*$^{G12V}$*p53*$^{-/-}$ mouse model via the induction of an activated stroma, increased angiogenesis, and inhibition of immune cell infiltration. Thus, targeting the Gal1–glycan axis may offer new therapeutic opportunities for PDA patients.

**Human PSCs Drive in Vitro Pancreatic Tumor Migration, Invasion, and Proliferation via Gal1.** To explore whether our findings using the *Kras*-driven PDA mouse model could be translated to human pathology and to gain further insights into the molecular mechanisms underlying Gal1 functions in pancreatic cancer, we designed a human cell-based experimental system to mirror tumor–stroma crosstalk. For this, we used immortalized PSCs isolated from human PDA samples (human pancreatic stellate cells; HPSCs) (14) that express high endogenous levels of Gal1 (43) and two human pancreatic tumor cell lines (RWP-1 and BxPC-3) with undetectable/low levels of Gal1 expression (42). Gal1 knockdown in HPSCs (Fig. S3 *A* and *B*) resulted in impaired cell activation, shown by reduced levels of fibroblast activation markers (Fig. S3 *C* and *D*), morphological changes (Fig. S3*E*), and decreased migration and invasion (Fig. S3 *G* and *H*), while not affecting cell proliferation (Fig. S3*F*). To investigate the paracrine effects of PSC-secreted Gal1 in PDA epithelial cells, we used conditioned medium from control or Gal1-knocked down (shGal1) HPSCs (Fig. 4 *A* and *B*) to treat RWP-1 cells. Remarkably, conditioned medium from control HPSCs (either untransfected or transfected with an irrelevant shRNA) induced proliferation, migration, and invasion in RWP-1 cells (Fig. 4 *C*–*E*), while these effects were significantly impaired when Gal1-depleted (shGal1) HPSC supernatant was used. Similar results were obtained using the BxPC-3 pancreatic tumor cell line (Fig. S4). Thus, HPSCs accentuate the tumorigenic capacity of pancreatic epithelial cells via paracrine secretion of Gal1.

**Human PSCs Drive in Vivo Pancreatic Tumor Progression via Gal1.** To further investigate the role of HPSC-derived Gal1 in pancreatic tumor–stroma crosstalk during in vivo cancer progression, we used a xenograft orthotopic model of PDA in which HPSCs, either stably depleted of Gal1 (shGal1) or transfected with a scrambled shRNA (shSC) sequence, and BxPC-3 pancreatic tumor cells were coinjected in a 5:1 ratio to mirror the high fibrotic component of human tumors. Xenografts from BxPC-3 cells alone were used as a negative control, and two different Gal1-specific shRNA sequences were used to rule out off-target effects (Fig. 5). As previously reported (14), we found that the stroma worked synergistically with pancreatic tumor cells to accelerate tumor progression. Specifically, tumors generated after coinjection of BxPC-3 cells with control HPSCs were larger than those injected with BxPC-3 cells alone (Fig. 5*A*). Remarkably, Gal1 depletion in the coinjected HPSCs significantly reduced tumor size to a magnitude similar to that of tumors generated with BxPC-3 cells alone (Fig. 5*A*). Histopathological analysis of the pancreatic tumors revealed large undifferentiated ductal tumors with central necrotic cores (Fig. 5*B*). Detailed immunohistochemical analysis showed no significant differences in tumor proliferation or angiogenesis (Fig. 5*C*). However, in line with results obtained in the *Kras*-driven mouse PDA model, tumors generated after coinjection of BxPC-3 cells with Gal1-depleted HPSCs exhibited a significant decrease in the amount of active stroma (Fig. 5*C*). Moreover, we also observed increased metastasis formation in mice coinjected with BxPC-3 cells and control HPSCs as compared with mice inoculated with BxPC-3 cells alone or coinjected with BxPC-3 tumor cells mixed with Gal1-depleted HPSCs (Fig. 5*D*). These findings support a role for HPSC-secreted Gal1 as one of the key mediators of the interplay between the stroma and the epithelium to promote in vivo tumor growth and progression in human PDA.

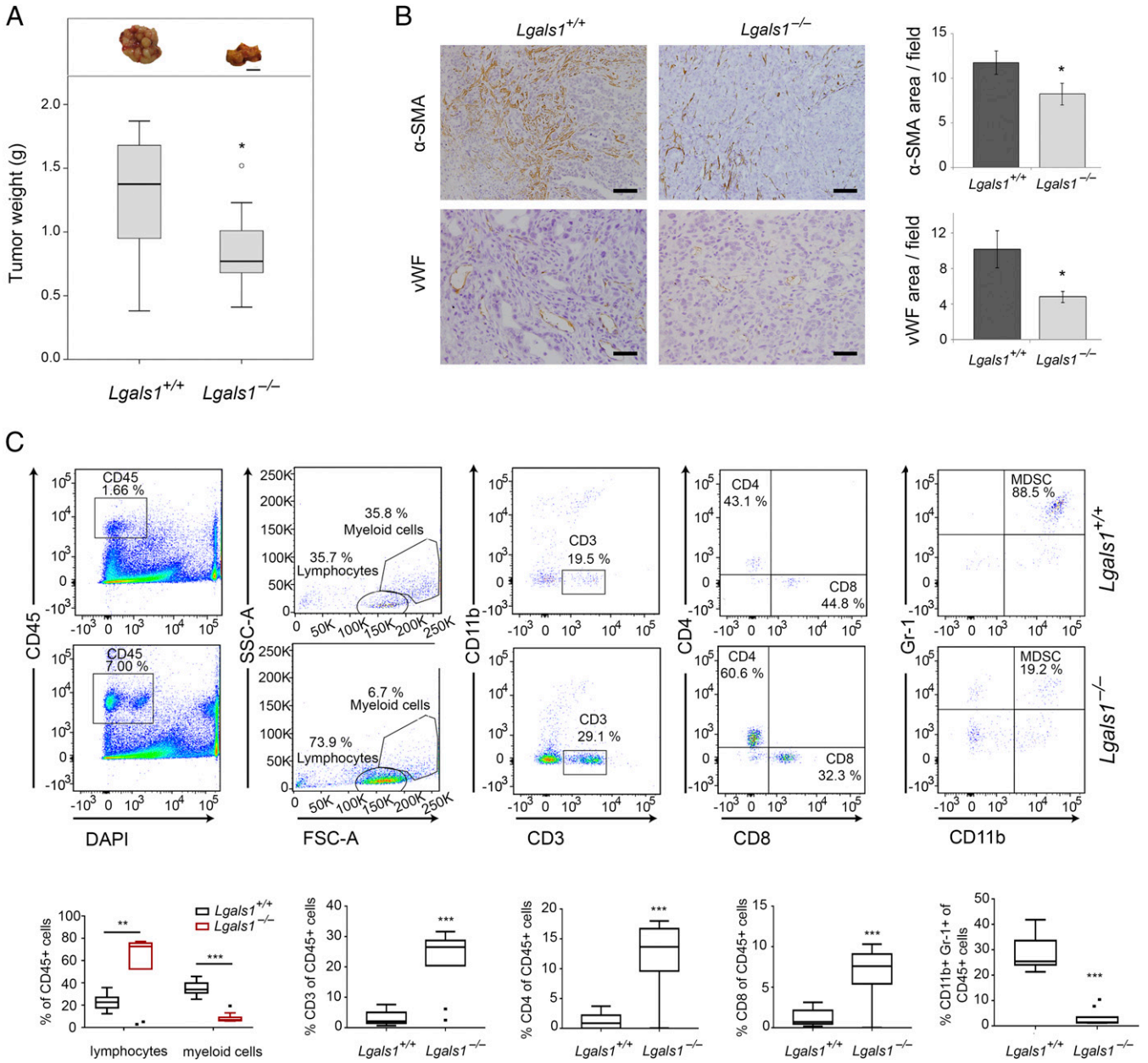


**Fig. 3.** Characterization of pancreatic tumors from 4-mo-old *Ela-Kras*$^{G12V}$*p53*$^{-/-}$*Lgals1*$^{+/+}$ and *Ela-Kras*$^{G12V}$*p53*$^{-/-}$*Lgals1*$^{-/-}$ mice. (*A*) Representative images (*Upper*) and box-and-whisker plots (*Lower*) showing the weights of pancreatic tumors from *Ela-Kras*$^{G12V}$*p53*$^{-/-}$*Lgals1*$^{+/+}$ and *Ela-Kras*$^{G12V}$*p53*$^{-/-}$*Lgals1*$^{-/-}$ mice. (Scale bars: 1 cm.) (*B*, *Left*) Histochemical analysis of activated stroma (α-SMA staining) and vascularization [von Willebrand factor (vWF) staining] of pancreatic tumors from *Ela-Kras*$^{G12V}$*p53*$^{-/-}$*Lgals1*$^{+/+}$ and *Ela-Kras*$^{G12V}$*p53*$^{-/-}$*Lgals1*$^{-/-}$ mice. (Scale bars: 100 μm for α-SMA and 50 μm for vWF.) (*Right*) Quantifications expressed as the percentage of α-SMA–stained area per field or the percentage of vWF staining relative to the number of tumor cells. **P* < 0.05. (*C*) Flow cytometry analysis of immune cell infiltrates associated with pancreatic tumors from *Ela-Kras*$^{G12V}$*p53*$^{-/-}$*Lgals1*$^{+/+}$ or *Ela-Kras*$^{G12V}$*p53*$^{-/-}$*Lgals1*$^{-/-}$ mice. Representative plots of tumor-infiltrating immune cells expressing CD45, CD3, CD4, and CD8 or CD11b and Gr-1 are shown. Percentages of cells of each individual subpopulation ($CD3^+CD4^+$ cells, $CD3^+CD8^+$ cells, and $CD11b^+Gr\text{-}1^+$ cells) are indicated. ***P* < 0.01, ****P* < 0.001 (Student's *t* test). Ten animals per group were used for the characterizations in *A*–*C*.

**Molecular Pathways Activated by Gal1 on Pancreatic Epithelial Cells.** To understand the molecular mechanisms underlying the paracrine effects exerted by stromal Gal1 on the pancreatic epithelial compartment, we performed a high-throughput analysis using microarrays. To specifically address Gal1-driven pathways, we avoided using conditioned medium from HPSCs (which may contain several secreted factors) and instead treated RWP-1 pancreatic tumoral cells with recombinant Gal1 (rGal1). The addition of rGal1 increased in vitro proliferation, migration, and invasion of RWP-1 cells (Fig. S5) similarly to our findings using HPSC conditioned medium. Gene-expression profiling using the GeneChip Human Gene 2.0 ST expression array revealed 339 genes differentially expressed between RWP-1 cells grown in basal conditions and cells treated with rGal1, of which 156 genes were up-regulated, and 183 genes were down-regulated (Fig. 6*A* and Dataset S1).

Gene ontology (GO) analysis of Gal1 target genes identified a significant enrichment in genes involved in tumor biology, including cell signaling, motility, morphology, inflammatory responses, immune cell trafficking, cell commitment, tumor morphology,

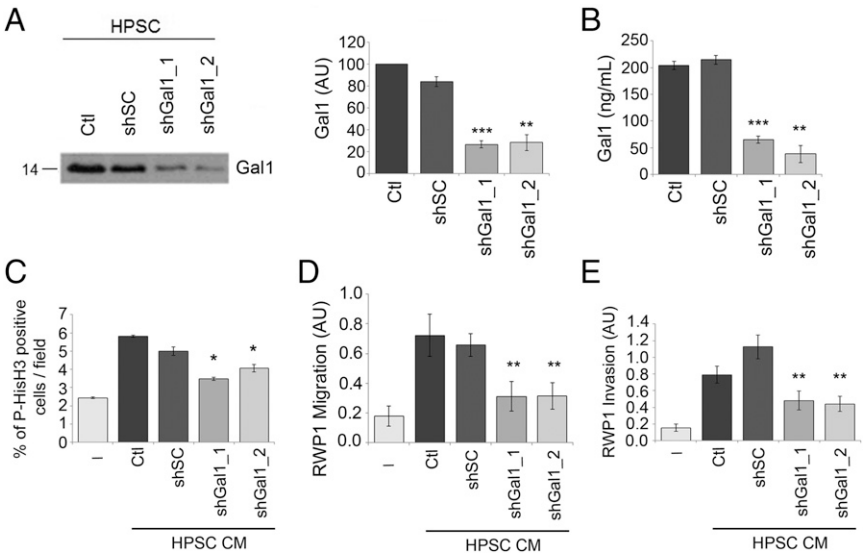


**Fig. 4.** Crosstalk between HPSCs and pancreatic tumor cells is mediated by HPSC-secreted Gal1. (*A*, *Left*) Western blot analysis of Gal1 protein expression levels in supernatants of control HPSCs (Ctl), cells infected with shSC, or cells infected with two different Gal1-specific sequences (shGal1_1 and shGal1_2). (*Right*) Quantification. (*B*) ELISA quantification of Gal1 levels in supernatants of HPSC control cells (Ctl) or shSC-, shGal1_1-, or shGal1_2-infected cells. (*C*) Effects of conditioned medium (CM) from Gal1-depleted HPSCs on RWP-1 cell proliferation using immunofluorescence against the P-HisH3 marker. (*D*) Effects of conditioned medium from Gal1-depleted HPSCs on RWP-1 migration using a Transwell assay. (*E*) Effects of conditioned medium from Gal1-depleted HPSCs on the invasion of RWP-1 cells through Matrigel-coated Transwells. Data are given as the mean ± SEM of three independent experiments. $*P < 0.05$ and $**P < 0.01$ relative to shSC.

and signaling pathways (Fig. 6*B*). Of note, Ingenuity Pathway Analysis showed associated network functions related to cellular motility, growth, and proliferation (Fig. 6*C*), which correlated well with the biological functions displayed by Gal1 in experimental mouse and human PDA models. Top disease analyses identified the most significant enrichment in cancer-related molecules, and biofunction classification distinguished the cell cycle, motility, morphology, assembly, and cell commitment pathways (Table S2).

To gain further insight into the molecular pathways driven by Gal1 in human pancreatic cancer, we selected several cancer-related candidates from the list of genes differentially expressed in RWP-1 cells after rGal1 treatment and validated their expression levels by RT-qPCR (Fig. 6*D*). Interestingly, exposure of RWP-1 cells to rGal1 resulted in a significant overexpression of genes involved in cell proliferation and metastasis (*IL1A* and *MMP1*), migration (*S100A7* and *ANK3*), cell metabolism (*EXTL2* and *GPCPD1*), and other pathways (*ASXL3*, *AGPAT9*, *GALNT16*, and *TOX*), as well as down-regulation of the Hedgehog (Hh) inhibitor *DHCR7*, the putative tumor-suppressor gene *INSIG1* (50), and other genes with uncertain roles in cancer (*TFRC*, *CLCNK8*, and *ROCK1*).

These findings identify gene networks that are directly or indirectly modulated by Gal1 in pancreatic epithelial tumor cells, thus providing a molecular perspective on the mechanisms involved in tumor–stroma crosstalk and their impact in pancreatic cancer progression.

## Discussion

Improving pancreatic cancer patients' outcome is an important unmet clinical need. Alarmingly, both its incidence and associated death rates are increasing, so that pancreatic cancer is now in the third position of the top cancer killers in the United States and is anticipated to become the second leading cause of cancer death by 2030 (51). To improve the currently bleak perspectives for most PDA patients, it is critical to identify new molecular targets for the development of effective treatments. Here, using a combination of GEMM- and human-based experimental systems, we provide evidence that inhibition of Gal1, a protein overexpressed by stromal fibroblasts, may hinder PDA tumor progression by impeding an efficient tumor–stroma crosstalk, thereby supporting the use of Gal1 inhibitors as a pharmacological weapon for the treatment of pancreatic cancer patients, either alone or in combination with immunotherapeutic, chemotherapeutic, or targeted strategies.

PDA is unique in its stromal composition, which frequently accounts for more than 90% of the tumor mass. In fact, this dense fibrotic barrier is considered one of the major reasons for PDA resistance to therapies (3, 52). Another key hallmark of PDA is *KRAS* mutations, which are present in >90% of PDA patients (24) and are essential for tumor initiation and progression (53, 54). Importantly, mouse *Kras*-driven models recapitulate not only these two features of human PDA but also its profound immunosuppression (33) and tumor genetic heterogeneity (55–60). These hallmarks strongly support the use of these mice for preclinical validation of novel targeted therapies. We previously reported a beneficial effect of Gal1 inhibition using a *c-myc*–driven PDA model (43); however, these mice did not fully recapitulate the tumor progression found in human disease (61). In contrast, the *Ela-Kras*$^{G12V}$*p53*$^{-/-}$ mice used in this work faithfully recapitulate the full spectrum of pancreatic intraepithelial neoplasias that progress to human-like PDA tumors and, like PDA patients, develop liver metastases (28, 48), thus making this model an ideal system for testing novel molecular targets. Using this *Kras*-driven model, we have found that genetic ablation of Gal1 increases animal survival and constrains tumor growth through multiple mechanisms involving decreased stroma activation and angiogenesis as well as augmented immune cell infiltration. Moreover, we demonstrated that Gal1 is involved not only in pancreatic tumor initiation but also at late stages of tumor progression, as shown by the reduction in liver metastases after Gal1 genetic deletion (Fig. 7). Remarkably, we also confirmed the induction of tumor progression and metastasis by stromal Gal1 using a human cell-based system that fully recapitulates Gal1-mediated tumor–stroma crosstalk in human PDA (Fig. 7), unveiling the potential translation of these results to PDA clinical setting.

Collectively, our studies in mouse and human settings indicate that pancreatic cancer stromal Gal1 exerts both autocrine and paracrine protumoral functions. First, Gal1 secreted by PSCs induces stroma activation through an autocrine loop. In this regard, previous data using different in vitro and in vivo models have shown Gal1-mediated activation of PSC by triggering the ERK or Hh signaling pathways (43, 62, 63), although further studies are required to elucidate whether these mechanisms are also responsible for Gal1 induction of stroma activation in the *Kras*-driven model. On the other hand, Gal1 orchestrates a paracrine crosstalk with epithelial cells to induce proliferation, migration, and invasion, as well as with endothelial and inflammatory cells to promote angiogenesis and immune cell inhibition. Of note, the induction of cell proliferation in tumor epithelial cells by Gal1 is observed only in the in vitro setting, suggesting that non–cell-autonomous mechanisms or differences in kinetics during the in vivo experiments may account for this discrepancy. Different molecular

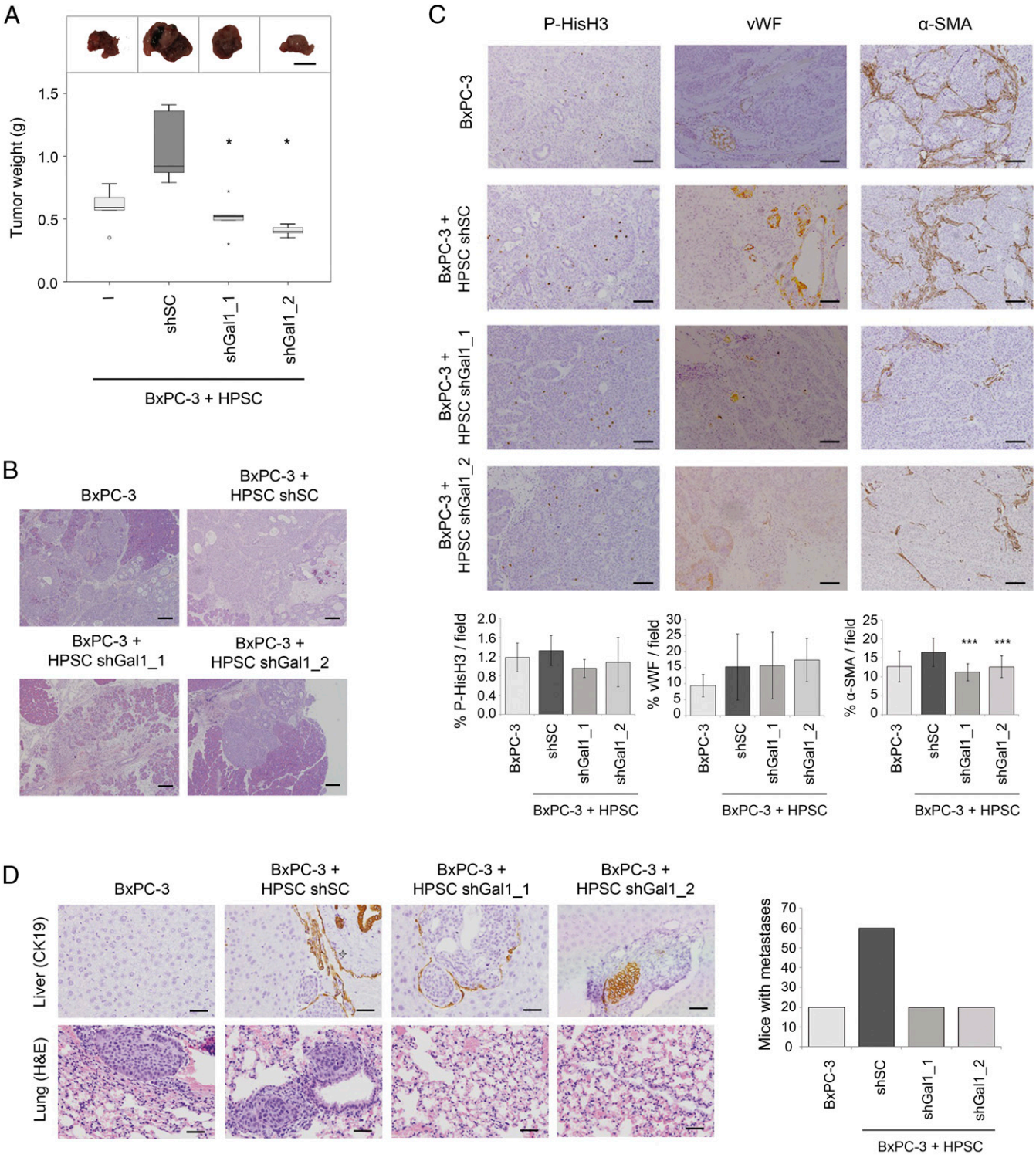


**Fig. 5.** Depletion of Gal1 in HPSCs reduces tumor size, angiogenesis, stroma activation, and metastasis after orthotopic coinjection with BxPC-3 pancreatic tumor cells. (*A*, *Upper*) A representative tumor for each group is shown. (Scale bars: 1 cm.) (*Lower*) Box-and-whisker plot representation of the tumor weight of orthotopic xenograft mice injected with BxPC-3 cells alone or with control HPSCs (shSC) or Gal1-knocked down (shGal1_1 and shGal1_2) HPSCs. $*P < 0.05$, relative to shSC. (*B*) Representative photographs of H&E-stained tumors in each group. Tumors display undifferentiated features and frequent necrotic areas. (Scale bars: 200 μm.) (*C*, *Upper*) Analysis of cell proliferation (P-HisH3 staining), vascularization (vWF staining), and activated stroma (α-SMA staining) in orthotopic xenografts tumors from mice injected with BxPC-3 cells alone or with HPSCs infected with shSC, shGal1_1, or shGal1_2. (Scale bars: 100 μm.) (*Lower*) Quantifications are expressed as the percentage of cells with P-HisH3$^+$ staining, the percentage of vWF staining relative to the number of tumor cells, and the percentage of α-SMA$^+$ area per field. $***P < 0.001$, relative to shSC. (*D*, *Left*) Representative images of pancreatic metastases using CK19 IHC staining (liver) or H&E staining (lung). (Scale bars: 50 μm.) (*Right*) Quantification of the percentage of mice with liver and lung metastases ($P = 0.20$, $\chi^2$ test).

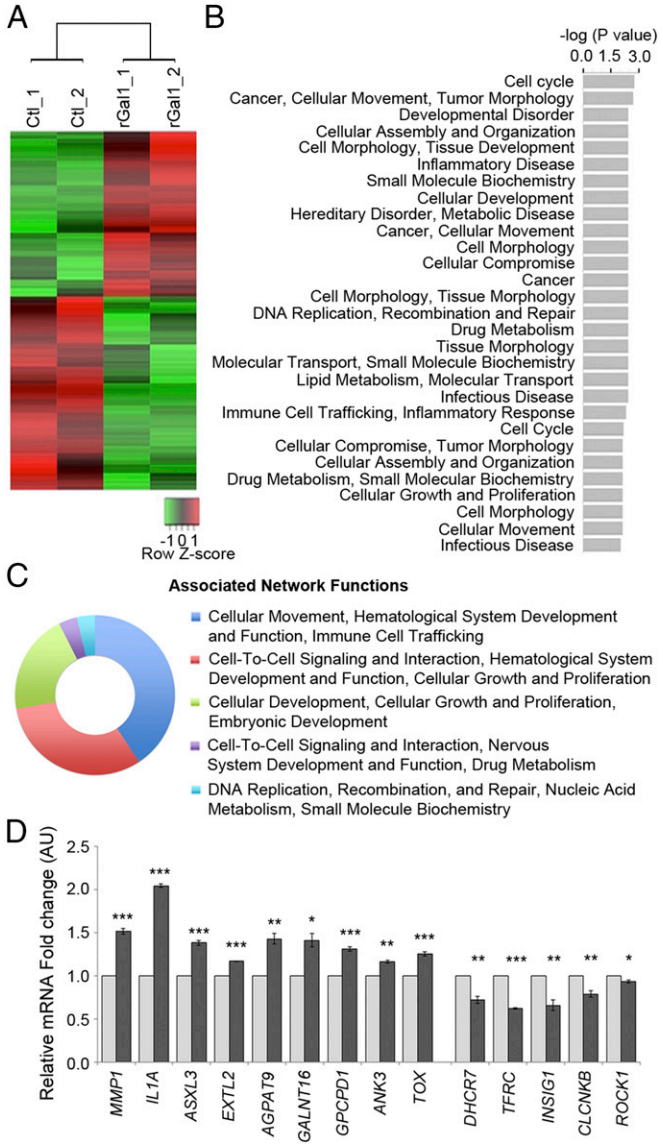


**Fig. 6.** Molecular pathways triggered by Gal1 in human pancreatic cancer. (*A*) Heatmap diagram of differential gene expression (with $P < 0.01$) in RWP-1 cells treated with rGal1 compared with untreated cells. (*B*) GO analysis of genes differentially expressed in RWP-1 cells after rGal1 treatment. The bar plot shows the $\log_{10}$ *P* value of the biological process GO terms obtained with differentially expressed genes with $P < 0.01$. (*C*) Ingenuity Pathway Analysis showing the top network functions of the genes regulated by rGal1 in RWP-1 cells. (*D*) RT-qPCR validation of gene-expression changes triggered by rGal1 treatment of pancreatic tumoral cells. Up-regulated or down-regulated genes found in the microarray analysis were validated by measuring the relative mRNA fold change by RT-qPCR in rGal1-treated cells (black bars) compared with untreated cells (control; gray bars). RNA levels were normalized using *GAPDH* as a housekeeping gene. Data are given as the mean ± SEM of three independent experiments. $*P < 0.05$; $**P < 0.005$; $***P < 0.0005$ (Student's *t* test).

mechanisms might be responsible for Gal1 paracrine functions. Microarray gene-expression analysis of human pancreatic tumor cells exposed to exogenous Gal1 revealed the prominent relevance of gene networks related to cell cycle, cellular migration, and tumor morphology among the top Gal1-regulated pathways, which might explain the effects of PSCs on epithelial tumor cells. In particular, we have validated the up-regulation of several target genes with previously established roles in PDA cell growth and invasion, such as *IL1A* and *MMP1* (64–66), as well as other genes involved in cell migration (i.e., *S100A7* and *ANK3*) (67, 68) and in cell growth and metastasis in other tumors (*TOX*) (69). Interestingly, we also found down-regulation of *DHCR7*, a negative regulator of the Hh signaling pathway (70), which is in agreement with our previous results showing that Gal1 mediates the activation of the Hh pathway in PDA cells, thereby promoting endothelial cell proliferation and migration (43). In this regard, a direct role of Gal1 in tumor angiogenesis has been well established (71–75), implicating this lectin as a critical mediator of hypoxia-driven and VEGF-independent angiogenesis (76). Interestingly, PDA displays a highly hypoxic microenvironment (77, 78) that could favor Gal1 overexpression (75, 76, 79). In addition, our microarray data suggest that Gal1 can also promote angiogenesis in PDA through an indirect mechanism mediated by the up-regulation of IL-1α, which might induce secretion of proangiogenic cytokines (80), or by the down-regulation of the transferrin receptor (TFRC), which may promote hypoxia and augment tumor angiogenesis (81). Moreover, aberrant N-glycosylation has been recently reported in human PDA cell lines compared with normal pancreatic cells (82), suggesting that glycan remodeling might promote the exposure of Gal1 ligands and regulate its biological function during tumor progression.

Interestingly, Gal1 deletion in the *Ela-Kras*$^{G12V}$*p53*$^{-/-}$ mice facilitated immune cell infiltration, indicating that this lectin has a

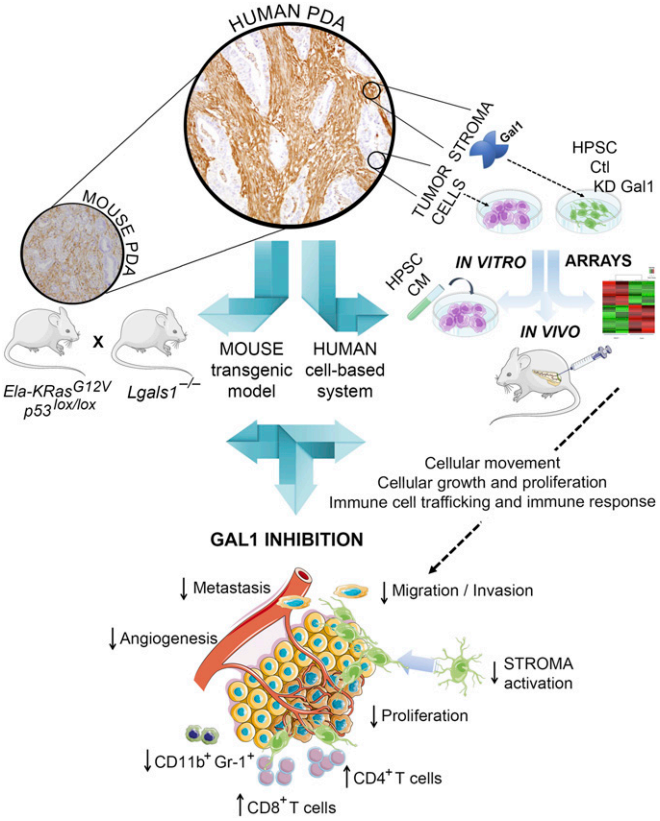


**Fig. 7.** Effects of Gal1 targeting in the control of pancreatic tumor progression. The role of Gal1 in pancreatic tumor progression was addressed in two experimental model systems: by genetically depleting Gal1 in the PDA model *Ela-Kras*$^{G12V}$*p53*$^{-/-}$ (*Left*) and by analyzing tumor–stroma crosstalk in a human-based in vitro system in which HPSCs with normal or down-regulated Gal1 levels (KD Gal1) were used for in vitro (CM) or in vivo (nude mice xenograft coinjection) strategies. Microarray analysis of pancreatic epithelial cells treated with rGal1 was also performed to depict the molecular scenario responsible for Gal1 effects on the epithelium. These data are summarized in the model, showing that Gal1 inhibition results in impaired migration, invasion, stroma activation, cell proliferation, angiogenesis, and metastasis while increasing tumor-immune infiltrates, ultimately leading to reduced tumor progression. Images adapted with permission from smart.servier.com.

critical role in impairing immune surveillance during PDA progression. In this sense, PDA is accompanied by a profound immunosuppressive microenvironment characterized by the accumulation of immature MDSCs and a conspicuous absence of tumor-infiltrating T lymphocytes, a scenario that is fully mimicked in the *Kras*-driven mouse models (33). This inhibitory milieu might explain why PDA patients do not respond to immune checkpoint-blockade therapies (23). Notwithstanding, recent genome-wide studies have identified molecular signatures (83) and unique neoantigen properties (84) that may be useful for stratifying PDA patients for immunotherapy. Data from murine PDA models have provided new mechanisms for PDA immunosuppression, showing that MDSCs can be recruited through *Kras*-driven paracrine secretion of GM-CSF by tumor cells (85, 86). Here, we demonstrate that Gal1 also plays a key role in MDSCs accumulation in *Kras*-driven PDA, as this regulatory cell population was dramatically reduced in *Ela-Kras* Gal1-KO mice. Accordingly, previous studies showed that Gal1 can promote the differentiation and selective retention of tolerogenic dendritic cells in inflamed tissues (87, 88) and may favor recruitment of MDSCs in a glioblastoma model (89). In parallel, we found that deletion of the Gal1 gene induces up-regulation of $CD4^+$ and $CD8^+$ T cell tumor infiltrates as shown in other tumor types, including melanoma (90), Hodgkin lymphoma (91), neuroblastoma (92), lung adenocarcinoma (93), ovary carcinoma (94), and breast adenocarcinoma (95). This effect may be directly related to T cell dysfunction induced by Gal1, as this lectin impairs T cell viability and suppresses the synthesis of T cell-derived proinflammatory cytokines (45, 96), or may involve the repression of regulatory circuits mediated by MDSCs or tolerogenic dendritic cells, leading to subsequent expansion of effector T cells (97). Interestingly, although $Lgals1^{-/-}$ mice did not originally show any overt phenotypic abnormality (98), more recent studies demonstrated that these animals develop more exacerbated immune responses when challenged by inflammatory or infectious stimuli (87, 96, 99, 100), suggesting that this lectin could be specifically targeted to augment T cell infiltration and reinvigorate antitumor immunity.

The pleiotropic functions exerted by Gal1 during PDA tumor progression suggest its potential role as an ideal therapeutic target. Gal1 inhibitors would simultaneously block the tumor and the stroma compartment, inhibiting tumor cell proliferation, vascularization, and fibroblast activation, while restoring immune surveillance. Thus, pharmacological inhibition of Gal1 or its glycosylated ligands using specific monoclonal antibodies, glycan inhibitors, or peptidomimetics could have a strong impact on PDA progression and contribute to enhancing the efficacy of currently available immunotherapeutic modalities. Interestingly Gal1-neutralizing antibodies have shown promising results in xenografts of Kaposi's sarcoma and syngeneic models of melanoma and lung cancer (75, 76).

In conclusion, our study validates Gal1 as a multifunctional target during PDA progression and paves the way toward the development of a new generation of drugs targeting the unique PDA microenvironment.

## Materials and Methods

**Animal Breeding and Use and Sample Collection.** *K-Ras*$^{+/LSLG12V}$;*Elas-tTA/tetO-Cre;p53*$^{lox/lox}$ mice were obtained from C. Guerra and M. Barbacid, Centro Nacional de Investigaciones Oncológicas (CNIO), Madrid (28, 48) and were crossed with Gal- KO ($Lgals1^{-/-}$) mice for Gal1 depletion in this model. *Ela-Kras*$^{G12V}$*p53*$^{-/-}$*Lgals1*$^{+/+}$ ($n$ = 18) and *Ela-Kras*$^{G12V}$*p53*$^{-/-}$*Lgals1*$^{-/-}$ ($n$ = 17) mice were killed at 4 mo of age for detailed histopathological characterization. For endpoint survival analysis, *Ela-Kras*$^{G12V}$*p53*$^{-/-}$*Lgals1*$^{+/+}$ ($n$ = 20) and *Ela-Kras*$^{G12V}$*p53*$^{-/-}$*Lgals1*$^{-/-}$ ($n$ = 19) mice were killed according to approved ethical guidelines when animal welfare was compromised. Pancreatic tumors, liver, and lungs were resected, weighed, fixed in 10% formaldehyde, and embedded in paraffin. All procedures were approved by the Barcelona Biomedical Research Park (PRBB) Ethical Committee for Animal Experimentation.

**Histopathological Assessment.** To screen for pancreatic precursor lesions or metastasis formation, paraffin-embedded full pancreata (precursor lesions) or livers and lungs (metastasis) were completely sliced. H&E staining was performed every 30 μm to screen for pancreatic lesions or foci of metastasis, which were all confirmed by an expert pathologist. Histological tissue parameters such as tumor architecture, desmoplasia, node infiltration, necrosis, apoptosis, and immune infiltration were analyzed under the supervision of an expert pathologist.

**Immunohistochemistry and Immunofluorescence.** Paraffin-embedded samples were cut at 3 μm for immunohistochemistry (IHC) analysis, as previously described (101), using the antibodies listed in *SI Materials and Methods*. Quantification was done by taking 10 images per tumor using an Olympus BX61 motorized microscope. Images were processed using ImageJ software (NIH) in which positively and negatively stained areas or cells were measured. Results are expressed as the percentage of positive area in each high-power field or the percentage of positive cells per field, where indicated. Immunofluorescence was performed as described (101) using the antibodies listed in *Supporting Information* and a Leica DM6000 digital microscope.

**Flow Cytometry of Tumor-Associated Immune Infiltrates.** Ten 4-mo-old mice per genotype were killed, and a piece of the resected pancreatic tumor was clipped and processed as previously described (33). Antibodies for blocking and surface labeling are listed in *Supporting Information*. For staining controls, unstained, fluorescence minus one (FMO), and individual stained controls were included for all surface-marker combinations. Cells were stained with DAPI (Sigma) and analyzed by FACS in a LSRII flow cytometer (BD Bioscience) at the Pompeu Fabra University (UPF) Flow Cytometry facility.

**Cell Lines.** HPSC were generated as previously described (14). HEK293T cells (102) and the human pancreatic ductal tumor cell lines RWP-1 (103) and BxPC-3 (104) were obtained from the cancer cell repository at Hospital del Mar Medical Research Institute (IMIM), Barcelona. Cells were cultured at 37 °C in a cell incubator at 5% $CO_2$ using DMEM (Gibco) with 10% FBS.

**Gal1 Down-Regulation in HPSCs.** shRNA-mediated Gal1 down-regulation was achieved with lentiviral particles generated in HEK-293T cells encoding the pLKO-1 vector, Mission RNAi, shGal1, TRCN0000057424,427 (Sigma), or control shSC (SHC002).

**Protein Lysates and Western Blot Analysis.** Total protein extracts were obtained by lysing cells in 1× Laemmli buffer (60 mM Tris-Cl pH 6.8, 2% SDS, 10% glycerol, 5% β-mercaptoethanol, 0.01% bromophenol blue). Protein expression was detected by SDS/PAGE under reducing conditions, and immunoblotting was performed with anti-Gal1 (Abcam), anti-fibronectin (Sigma), anti-GFAP (Sigma), anti–α-SMA (Sigma), anti-GAPDH (Abcam), and anti-tubulin (Sigma) antibodies. HRP-conjugated secondary antibodies (Dako) followed by ECL (Thermo Fisher) incubation allowed protein band detection.

**Preparation of HPSC-Conditioned Medium.** HPSCs were cultured in 75-$cm^2$ flasks with DMEM and 10% FBS. Upon 80% confluence, cells were left with 4 mL of serum-free DMEM, and secreted factors were collected after 48 h. Gal1 protein was quantified by ELISA (R&D Systems).

**Cell Proliferation Assay.** For HPSCs proliferation assays, 3-[4,5-dimethylthiazol-2-yl]-2,5-diphenyltetrazolium bromide] (MTT) staining was performed as described (101). For tumor–stroma crosstalk and proliferation assays using rGal1 (105), cells were starved for 48 h and stimulated with conditioned medium from HPSCs or rGal1 for 24 h. Cell proliferation was measured by phospho-histone H3 (P-HisH3) staining (see *Immunofluorescence* above). Twenty photographs at 20× magnification were taken, and proliferation was measured using ImageJ software quantifying the ratio between P-$HisH3^+$ cells and the total number of cells (DAPI).

**Migration Assays.** To evaluate migration in HPSCs, wound healing was performed as described (42). For tumor–stroma crosstalk experiments, epithelial cells were seeded in 96-well Transwells (8 μm; Corning). Conditioned medium from HPSCs or DMEM as a negative control was added to the lower chamber, and migration was assessed after 72 h by quantifying cells through hexosaminidase enzymatic substrate uptake and absorbance at 410 nm in a spectrophotometer (200 series; Tecan). For experiments using rGal1, a cell radius migration assay kit (Cell Biolabs) was used following the manufacturer's instructions. Images of the gap closure were taken with a bright-light microscope, and the covered area was quantified using ImageJ software.

**Invasion Assays.** Cells were seeded in Matrigel-coated 96-well Transwells (8 μm; Corning). DMEM with 10% FBS, conditioned medium from HPSCs (for tumor–stroma crosstalk assays), rGal1, or DMEM as a negative control was added to the lower chamber. Cells that invaded to the bottom layer were quantified by hexosaminidase enzymatic substrate uptake after 72 h.

**Orthotopic Coinjection in BALB/C Nude Mice.** Pancreatic orthotopic injection was performed following the guidelines described by Kim et al. (106), using 7-wk-old BALB/c nude mice (Charles River; five mice per group). BxPC-3 cells and HPSCs were injected at a 1:5 ratio ($4 \times 10^5$ and $2 \times 10^6$ cells, respectively). Tumors were monitored once a week for 5 wk; then all animals were killed.

**Reverse Transcription and Real-Time qPCR Analysis.** RNA was isolated using the total RNA extraction kit (Sigma) or the RNeasy Plus Mini kit (Qiagen) for microarray analysis. RNA was analyzed in a NanoDrop ND-1000 spectrophotometer (NanoDrop Technologies) and a Bioanalyzer 2100 (Agilent Technologies). RNA was retro-transcribed (RevertAid First Strand cDNA Synthesis Kit; Thermo Scientific). Human *HPRT* and *GAPDH* were used as housekeeping genes. qRT-PCR ($n = 3$) was performed by SYBR Green on the QuantStudio Real-Time PCR System (Life Technologies) using the primers listed in Table S3.

**Microarray Analysis and Bioinformatics.** Microarray samples were processed according to the protocol described in the GeneChip WT PLUS Reagent Kit and then hybridized to GeneChip Human Gene 2.0 ST Array (Affymetrix) in a GeneChip Hybridization Oven 640. Details and computational analysis are described in *Supporting Information*. Data have been deposited in the National Center for Biotechnology Information Gene Expression Omnibus (GEO) with the GEO Series accession number GSE109070.

**Statistical Analysis.** Data analyses were carried out using SPSS statistics version 20 software (IBM). $P < 0.05$ was considered statistically significant (*$P < 0.05$; **$P < 0.01$; ***$P < 0.001$). Unless otherwise stated, all data are expressed as the relative mean of three independent experiments, and error bars indicate the SEM. Comparisons were made through Student's $t$ test for normally distributed data; $\chi^2$ was used to analyze metastasis data. Kaplan–Meier survival analysis and a log-rank test were used to plot mouse survival.

**ACKNOWLEDGMENTS.** We thank J. M. Caballero (PRBB Animal Facility) and the staffs of the UPF Flow Cytometry and the IMIM microarray core facilities for helpful technical assistance, Raul Peña and the Epithelial-to-Mesenchymal Transition and Cancer Progression group (IMIM) for providing reagents and valuable technical help, and V. A. Raker for English proofreading and manuscript editing. Images for figure preparation were provided by SMART (Servier Medical Art, https://smart.servier.com/). This work was supported by Spanish Ministry of Economy and Competitiveness/ISCIII-FEDER Grants PI14/00125 and PI17/00199, the Carmen Delgado/Miguel Pérez-Mateo Asociación Española de Pancreatología/ Asociación Cáncer de Páncreas 2016 Grant, and Generalitat de Catalunya Grant 2014/SGR/143 (to P.N.). M.E.F.-Z. was supported by Mayo Clinic Pancreatic Specialized Program of Research Excellence Grant P50 CA102701 and Mayo Clinic Center for Cell Signaling in Gastroenterology Grant P30 DK84567. C.A.O. was supported by the International PhD Studies Fellowship Créditos Beca Francisco José de Caldas from the Colombian Administrative Department of Science, Technology and Innovation (Colciencias). M.D. was supported by a fellowship from La Caixa International Fellowship Program. G.A.R. was supported by Argentinean Agency for Promotion of Science and Technology Grant PICT 2014-3687 and by grants from the University of Buenos Aires, the Sales Foundation, and the Bunge and Born Foundation. T.D.-M. is a postdoctoral fellow supported by the Argentine National Scientific and Technical Research Council.

1. Rahib L, et al. (2014) Projecting cancer incidence and deaths to 2030: The unexpected burden of thyroid, liver, and pancreas cancers in the United States. *Cancer Res* 74: 2913–2921.
2. Hidalgo M (2010) Pancreatic cancer. *N Engl J Med* 362:1605–1617.
3. Neesse A, et al. (2011) Stromal biology and therapy in pancreatic cancer. *Gut* 60: 861–868.
4. Olive KP, et al. (2009) Inhibition of hedgehog signaling enhances delivery of chemotherapy in a mouse model of pancreatic cancer. *Science* 324:1457–1461.
5. Provenzano PP, et al. (2012) Enzymatic targeting of the stroma ablates physical barriers to treatment of pancreatic ductal adenocarcinoma. *Cancer Cell* 21:418–429.
6. Jacobetz MA, et al. (2013) Hyaluronan impairs vascular function and drug delivery in a mouse model of pancreatic cancer. *Gut* 62:112–120.
7. Sherman MH, et al. (2014) Vitamin D receptor-mediated stromal reprogramming suppresses pancreatitis and enhances pancreatic cancer therapy. *Cell* 159:80–93.
8. Froeling FE, et al. (2011) Retinoic acid-induced pancreatic stellate cell quiescence reduces paracrine Wnt-β-catenin signaling to slow tumor progression. *Gastroenterology* 141:1486–1497.
9. Rhim AD, et al. (2014) Stromal elements act to restrain, rather than support, pancreatic ductal adenocarcinoma. *Cancer Cell* 25:735–747.
10. Özdemir BC, et al. (2014) Depletion of carcinoma-associated fibroblasts and fibrosis induces immunosuppression and accelerates pancreas cancer with reduced survival. *Cancer Cell* 25:719–734.
11. Bijlsma MF, van Laarhoven HWM (2015) The conflicting roles of tumor stroma in pancreatic cancer and their contribution to the failure of clinical trials: A systematic review and critical appraisal. *Cancer Metastasis Rev* 34:97–114.
12. Lee JJ, et al. (2014) Stromal response to hedgehog signaling restrains pancreatic cancer progression. *Proc Natl Acad Sci USA* 111:E3091–E3100.
13. Bachem MG, et al. (2005) Pancreatic carcinoma cells induce fibrosis by stimulating proliferation and matrix synthesis of stellate cells. *Gastroenterology* 128:907–921.
14. Hwang RF, et al. (2008) Cancer-associated stromal fibroblasts promote pancreatic tumor progression. *Cancer Res* 68:918–926.
15. Vonlaufen A, et al. (2008) Pancreatic stellate cells and pancreatic cancer cells: An unholy alliance. *Cancer Res* 68:7707–7710.
16. Xu Z, et al. (2010) Role of pancreatic stellate cells in pancreatic cancer metastasis. *Am J Pathol* 177:2585–2596.
17. Moir JAG, Mann J, White SA (2015) The role of pancreatic stellate cells in pancreatic cancer. *Surg Oncol* 24:232–238.
18. Tang D, et al. (2013) Persistent activation of pancreatic stellate cells creates a microenvironment favorable for the malignant behavior of pancreatic ductal adenocarcinoma. *Int J Cancer* 132:993–1003.
19. Djurec M, et al. (2018) Saa3 is a key mediator of the protumorigenic properties of cancer-associated fibroblasts in pancreatic tumors. *Proc Natl Acad Sci USA* 115: E1147–E1156.
20. von Bernstorff W, et al. (2001) Systemic and local immunosuppression in pancreatic cancer patients. *Clin Cancer Res* 7:925s–932s.
21. Hiraoka N, Onozato K, Kosuge T, Hirohashi S (2006) Prevalence of FOXP3+ regulatory T cells increases during the progression of pancreatic ductal adenocarcinoma and its premalignant lesions. *Clin Cancer Res* 12:5423–5434.
22. Koido S, et al. (2011) Current immunotherapeutic approaches in pancreatic cancer. *Clin Dev Immunol* 2011:267539.
23. Martinez-Bosch N, Vinaixa J, Navarro P (2018) Immune evasion in pancreatic cancer: From mechanisms to therapy. *Cancers (Basel)* 10:E6.
24. Almoguera C, et al. (1988) Most human carcinomas of the exocrine pancreas contain mutant c-K-ras genes. *Cell* 53:549–554.
25. Hruban RH, Wilentz RE, Kern SE (2000) Genetic progression in the pancreatic ducts. *Am J Pathol* 156:1821–1825.
26. Drosten M, Guerra C, Barbacid M (2017) Genetically engineered mouse models of K-Ras-driven lung and pancreatic tumors: Validation of therapeutic targets. *Cold Spring Harb Perspect Med*, 10.1101/cshperspect.a031542.
27. Hingorani SR, et al. (2003) Preinvasive and invasive ductal pancreatic cancer and its early detection in the mouse. *Cancer Cell* 4:437–450.
28. Guerra C, et al. (2011) Pancreatitis-induced inflammation contributes to pancreatic cancer by inhibiting oncogene-induced senescence. *Cancer Cell* 19:728–739.
29. Gidekel Friedlander SY, et al. (2009) Context-dependent transformation of adult pancreatic cells by oncogenic K-Ras. *Cancer Cell* 16:379–389.
30. Habbe N, et al. (2008) Spontaneous induction of murine pancreatic intraepithelial neoplasia (mPanIN) by acinar cell targeting of oncogenic Kras in adult mice. *Proc Natl Acad Sci USA* 105:18913–18918.
31. Carriere C, Seeley ES, Goetze T, Longnecker DS, Korc M (2007) The Nestin progenitor lineage is the compartment of origin for pancreatic intraepithelial neoplasia. *Proc Natl Acad Sci USA* 104:4437–4442.
32. De La OJ-P, et al. (2008) Notch and Kras reprogram pancreatic acinar cells to ductal intraepithelial neoplasia. *Proc Natl Acad Sci USA* 105:18907–18912.
33. Clark CE, et al. (2007) Dynamics of the immune reaction to pancreatic cancer from inception to invasion. *Cancer Res* 67:9518–9527.
34. Compagno D, et al. (2014) Galectins: Major signaling modulators inside and outside the cell. *Curr Mol Med* 14:630–651.
35. Rabinovich GA, Conejo-García JR (2016) Shaping the immune landscape in cancer by galectin-driven regulatory pathways. *J Mol Biol* 428:3266–3281.
36. Kaltner H, et al. (2017) Galectins: Their network and roles in immunity/tumor growth control. *Histochem Cell Biol* 147:239–256.
37. Camby I, Le Mercier M, Lefranc F, Kiss R (2006) Galectin-1: A small protein with major functions. *Glycobiology* 16:137R–157R.
38. Martinez-Bosch N, Navarro P (2012) Glycans and galectins: Sweet new approaches in pancreatic cancer diagnosis and treatment. *Pancreatic Cancer: Molecular Mechanism and Targets*, ed Srivastava SK (InTech, Rijeka, Croatia), pp 305–328.
39. Berberat PO, et al. (2001) Comparative analysis of galectins in primary tumors and tumor metastasis in human pancreatic cancer. *J Histochem Cytochem* 49:539–549.
40. Iacobuzio-Donahue CA, et al. (2003) Highly expressed genes in pancreatic ductal adenocarcinomas: A comprehensive characterization and comparison of the transcription profiles obtained from three major technologies. *Cancer Res* 63:8614–8622.
41. Shen J, Person MD, Zhu J, Abbruzzese JL, Li D (2004) Protein expression profiles in pancreatic adenocarcinoma compared with normal pancreatic tissue and tissue affected by pancreatitis as detected by two-dimensional gel electrophoresis and mass spectrometry. *Cancer Res* 64:9018–9026.
42. Roda O, et al. (2009) Galectin-1 is a novel functional receptor for tissue plasminogen activator in pancreatic cancer. *Gastroenterology* 136:1375–1379.
43. Martinez-Bosch N, et al. (2014) Galectin-1 drives pancreatic carcinogenesis through stroma remodeling and hedgehog signaling activation. *Cancer Res* 74:3512–3524.
44. Xue X, et al. (2011) Galectin-1 secreted by activated stellate cells in pancreatic ductal adenocarcinoma stroma promotes proliferation and invasion of pancreatic cancer

cells: An in vitro study on the microenvironment of pancreatic ductal adenocarcinoma. *Pancreas* 40:832–839.
45. Tang D, et al. (2015) Apoptosis and anergy of T cell induced by pancreatic stellate cells-derived galectin-1 in pancreatic cancer. *Tumour Biol* 36:5617–5626.
46. Qian D, et al. (2017) Galectin-1-driven upregulation of SDF-1 in pancreatic stellate cells promotes pancreatic cancer metastasis. *Cancer Lett* 397:43–51.
47. Tang D, et al. (2017) PSC-derived Galectin-1 inducing epithelial-mesenchymal transition of pancreatic ductal adenocarcinoma cells by activating the NF-κB pathway. *Oncotarget* 8:86488–86502.
48. Guerra C, et al. (2007) Chronic pancreatitis is essential for induction of pancreatic ductal adenocarcinoma by K-Ras oncogenes in adult mice. *Cancer Cell* 11:291–302.
49. Méndez-Huergo SP, Blidner AG, Rabinovich GA (2017) Galectins: Emerging regulatory checkpoints linking tumor immunity and angiogenesis. *Curr Opin Immunol* 45:8–15.
50. Kaneda A, Kaminishi M, Nakanishi Y, Sugimura T, Ushijima T (2002) Reduced expression of the insulin-induced protein 1 andp41 Arp2/3 complex genes in human gastric cancers. *Int J Cancer* 100:57–62.
51. American Cancer Society (2017) *Cancer Facts & Figures 2017* (American Cancer Society, Atlanta).
52. Provenzano PP, Hingorani SR (2013) Hyaluronan, fluid pressure, and stromal resistance in pancreas cancer. *Br J Cancer* 108:1–8.
53. Collins MA, et al. (2012) Oncogenic Kras is required for both the initiation and maintenance of pancreatic cancer in mice. *J Clin Invest* 122:639–653.
54. Ying H, et al. (2012) Oncogenic Kras maintains pancreatic tumors through regulation of anabolic glucose metabolism. *Cell* 149:656–670.
55. Chung W-J, et al. (2017) *Kras* mutant genetically engineered mouse models of human cancers are genomically heterogeneous. *Proc Natl Acad Sci USA* 114: E10947–E10955.
56. Jones S, et al. (2008) Core signaling pathways in human pancreatic cancers revealed by global genomic analyses. *Science* 321:1801–1806.
57. Biankin AV, et al. (2012) Pancreatic cancer genomes reveal aberrations in axon guidance pathway genes. *Nature* 491:399–405.
58. Waddell N, et al. (2015) Whole genomes redefine the mutational landscape of pancreatic cancer. *Nature* 518:495–501.
59. Kugel S, et al. (2016) SIRT6 suppresses pancreatic cancer through control of Lin28b. *Cell* 165:1401–1415.
60. Witkiewicz AK, et al. (2015) Whole-exome sequencing of pancreatic cancer defines genetic diversity and therapeutic targets. *Nat Commun* 6:6744.
61. Sandgren EP, Quaife CJ, Paulovich AG, Palmiter RD, Brinster RL (1991) Pancreatic tumor pathogenesis reflects the causative genetic lesion. *Proc Natl Acad Sci USA* 88:93–97.
62. Fitzner B, et al. (2005) Galectin-1 is an inductor of pancreatic stellate cell activation. *Cell Signal* 17:1240–1247.
63. Masamune A, et al. (2006) Galectin-1 induces chemokine production and proliferation in pancreatic stellate cells. *Am J Physiol Gastrointest Liver Physiol* 290: G729–G736.
64. Sawai H, et al. (2003) Enhancement of integrins by interleukin-1alpha, and their relationship with metastatic and invasive behavior of human pancreatic ductal adenocarcinoma cells. *J Surg Oncol* 82:51–56.
65. Ottaviano AJ, Sun L, Ananthanarayanan V, Munshi HG (2006) Extracellular matrix–mediated membrane-type 1 matrix metalloproteinase expression in pancreatic ductal cells is regulated by transforming growth factor-β1. *Cancer Res* 66:7032–7040.
66. Shields MA, Dangi-Garimella S, Krantz SB, Bentrem DJ, Munshi HG (2011) Pancreatic cancer cells respond to type I collagen by inducing snail expression to promote membrane type 1 matrix metalloproteinase-dependent collagen invasion. *J Biol Chem* 286:10495–10504.
67. Padilla L, et al. (2017) S100A7: From mechanism to cancer therapy. *Oncogene* 36: 6749–6761.
68. Bourguignon LY, Zhu H, Shao L, Chen YW (2000) Ankyrin-Tiam1 interaction promotes Rac1 signaling and metastatic breast tumor cell invasion and migration. *J Cell Biol* 150:177–191.
69. Yu X, Li Z (2015) TOX gene: A novel target for human cancer gene therapy. *Am J Cancer Res* 5:3516–3524.
70. Koide T, Hayata T, Cho KWY (2006) Negative regulation of hedgehog signaling by the cholesterogenic enzyme 7-dehydrocholesterol reductase. *Development* 133: 2395–2405.
71. Thijssen VL, et al. (2006) Galectin-1 is essential in tumor angiogenesis and is a target for antiangiogenesis therapy. *Proc Natl Acad Sci USA* 103:15975–15980.
72. Thijssen VL, et al. (2010) Tumor cells secrete galectin-1 to enhance endothelial cell activity. *Cancer Res* 70:6216–6224.
73. Mathieu V, et al. (2012) Galectin-1 in melanoma biology and related neoangiogenesis processes. *J Invest Dermatol* 132:2245–2254.
74. Laderach DJ, et al. (2013) A unique galectin signature in human prostate cancer progression suggests galectin-1 as a key target for treatment of advanced disease. *Cancer Res* 73:86–96.
75. Croci DO, et al. (2012) Disrupting galectin-1 interactions with N-glycans suppresses hypoxia-driven angiogenesis and tumorigenesis in Kaposi's sarcoma. *J Exp Med* 209: 1985–2000.
76. Croci DO, et al. (2014) Glycosylation-dependent lectin-receptor interactions preserve angiogenesis in anti-VEGF refractory tumors. *Cell* 156:744–758.
77. Koong AC, et al. (2000) Pancreatic tumors show high levels of hypoxia. *Int J Radiat Oncol Biol Phys* 48:919–922.
78. Guillaumond F, et al. (2013) Strengthened glycolysis under hypoxia supports tumor symbiosis and hexosamine biosynthesis in pancreatic adenocarcinoma. *Proc Natl Acad Sci USA* 110:3919–3924.
79. Le Q-T, et al. (2005) Galectin-1: A link between tumor hypoxia and tumor immune privilege. *J Clin Oncol* 23:8932–8941.
80. Lewis AM, Varghese S, Xu H, Alexander HR (2006) Interleukin-1 and cancer progression: The emerging role of interleukin-1 receptor antagonist as a novel therapeutic agent in cancer treatment. *J Transl Med* 4:48.
81. Jones DT, Trowbridge IS, Harris AL (2006) Effects of transferrin receptor blockade on cancer cell proliferation and hypoxia-inducible factor function and their differential regulation by ascorbate. *Cancer Res* 66:2749–2756.
82. Holst S, Belo AI, Giovannetti E, van Die I, Wuhrer M (2017) Profiling of different pancreatic cancer cells used as models for metastatic behaviour shows large variation in their N-glycosylation. *Sci Rep* 7:16623.
83. Bailey P, et al. (2016) Genomic analyses identify molecular subtypes of pancreatic cancer. *Nature* 531:47–52.
84. Balachandran VP, et al. (2017) Identification of unique neoantigen qualities in long-term survivors of pancreatic cancer. *Nature* 551:512–516.
85. Bayne LJ, et al. (2012) Tumor-derived granulocyte-macrophage colony-stimulating factor regulates myeloid inflammation and T cell immunity in pancreatic cancer. *Cancer Cell* 21:822–835.
86. Pylayeva-Gupta Y, Lee KE, Hajdu CH, Miller G, Bar-Sagi D (2012) Oncogenic Kras-induced GM-CSF production promotes the development of pancreatic neoplasia. *Cancer Cell* 21:836–847.
87. Ilarregui JM, et al. (2009) Tolerogenic signals delivered by dendritic cells to T cells through a galectin-1-driven immunoregulatory circuit involving interleukin 27 and interleukin 10. *Nat Immunol* 10:981–991.
88. Thiemann S, Man JH, Chang MH, Lee B, Baum LG (2015) Galectin-1 regulates tissue exit of specific dendritic cell populations. *J Biol Chem* 290:22662–22677.
89. Verschuere T, et al. (2014) Glioma-derived galectin-1 regulates innate and adaptive antitumor immunity. *Int J Cancer* 134:873–884.
90. Rubinstein N, et al. (2004) Targeted inhibition of galectin-1 gene expression in tumor cells results in heightened T cell-mediated rejection; A potential mechanism of tumor-immune privilege. *Cancer Cell* 5:241–251.
91. Juszczynski P, et al. (2007) The AP1-dependent secretion of galectin-1 by Reed Sternberg cells fosters immune privilege in classical Hodgkin lymphoma. *Proc Natl Acad Sci USA* 104:13134–13139.
92. Soldati R, et al. (2012) Neuroblastoma triggers an immunoevasive program involving galectin-1-dependent modulation of T cell and dendritic cell compartments. *Int J Cancer* 131:1131–1141.
93. Banh A, et al. (2011) Tumor galectin-1 mediates tumor growth and metastasis through regulation of T-cell apoptosis. *Cancer Res* 71:4423–4431.
94. Rutkowski MR, et al. (2015) Microbially driven TLR5-dependent signaling governs distal malignant progression through tumor-promoting inflammation. *Cancer Cell* 27:27–40.
95. Dalotto-Moreno T, et al. (2013) Targeting galectin-1 overcomes breast cancer-associated immunosuppression and prevents metastatic disease. *Cancer Res* 73: 1107–1117.
96. Toscano MA, et al. (2007) Differential glycosylation of TH1, TH2 and TH-17 effector cells selectively regulates susceptibility to cell death. *Nat Immunol* 8:825–834.
97. Tesone AJ, et al. (2016) Satb1 overexpression drives tumor-promoting activities in cancer-associated dendritic cells. *Cell Rep* 14:1774–1786.
98. Poirier F, Robertson EJ (1993) Normal development of mice carrying a null mutation in the gene encoding the L14 S-type lectin. *Development* 119:1229–1236.
99. Blois SM, et al. (2007) A pivotal role for galectin-1 in fetomaternal tolerance. *Nat Med* 13:1450–1457.
100. Poncini CV, et al. (2015) *Trypanosoma cruzi* infection imparts a regulatory program in dendritic cells and T cells via galectin-1–dependent mechanisms. *J Immunol* 195: 3311–3324.
101. Martínez-Bosch N, et al. (2016) The pancreatic niche inhibits the effectiveness of sunitinib treatment of pancreatic cancer. *Oncotarget* 7:48265–48279.
102. Pear WS, Nolan GP, Scott ML, Baltimore D (1993) Production of high-titer helper-free retroviruses by transient transfection. *Proc Natl Acad Sci USA* 90:8392–8396.
103. Dexter DL, et al. (1982) Establishment and characterization of two human pancreatic cancer cell lines tumorigenic in athymic mice 1. *Cancer Res* 42:2705–2714.
104. Tan MH, et al. (1986) Characterization of a new primary human pancreatic tumor line 2. *Cancer Invest* 4:15–23.
105. Vértesy S, et al. (2015) Structural significance of galectin design: Impairment of homodimer stability by linker insertion and partial reversion by ligand presence. *Protein Eng Des Sel* 28:199–210.
106. Kim MP, et al. (2009) Generation of orthotopic and heterotopic human pancreatic cancer xenografts in immunodeficient mice. *Nat Protoc* 4:1670–1680.